AGU PUBLICATIONS

Tectonics

Supporting Information for

Seismicity induced at the northern Dead Sea Transform Fault, Kinneret (Sea of Galilee) Basin, by shallow creep involving a salt body

O. Barnea Cohen1, S. Cesca2, T. Dahm2, A. Hofstetter3, Y. Hamiel4, and A. Agnon1

[1]Neev Center for Geoinfomatics, Institute of Earth Sciences, The Hebrew University, Jerusalem 91904, Israel.

[2]GFZ German Research Center for Geoscience Potsdam, Telegrafenberg, 14473, Potsdam 14467, Germany.

[3]Independent researcher.

[4]Geological Hazards Division, Geological Survey of Israel, Jerusalem, Israel

Corresponding author: Osnat Barnea Cohen (osnat.barnea@mail.huji.ac.il)

Contents of this file

Introduction

This supporting information provides: **(a)**. The full relocation data of the October 2013 and 2018 clusters using Grigoli et al.'s (2013) method. **(b)** Table of the point source parameters for the seven largest earthquakes using Cesca et al.'s (2010) method. **(c)** Point source calculations of the largest 4th of July 2018 earthquakes. The stages of solutions are shown. **(c) -** Comparison of hypocentral depths using different velocity models and epicenter locations. **(d)** - Examples of earthquakes from two near-source borehole stations. **(e)** – Point source parameter solutions using the Double-couple method and moment tensor inversion (Heimann et al., 2018) with different velocity models (e.g., Gitterman et al., 2002; Haddad et al., 2020). **(f)** - Coulomb stress change model considering accumulated slip on the Jordan Valley Fault since the 1759 CE earthquake.

No.	Date	Time (hour: minute: second)	Location		Depth (km)	misfit
			Lat. (°N)	Long. (°E)		
1	17 October 2013	18:17:53.29	32.8648	35.6036	0.2	0.621
2	17 October 2013	18:20:06.42	32.8335	35.5033	0.2	0.441
3	17 October 2013	19:30:55.73	32.8125	35.5604	1.2	0.423
4	18 October 2013	02:01:59.20	32.8649	35.6004	0.2	0.44
5	18 October 2013	23:30:30.30	32.8559	35.5969	0.2	0.538
6	19 October 2013	04:37:46.88	32.9023	35.6667	0.9	0.335
7	19 October 2013	05:34:17.49	32.7503	35.5128	2.5	0.327
8	20 October 2013	05:19:40.66	32.7527	35.4872	10	0.372
9	20 October 2013	05:39:09.51	32.813	35.49	4.3	0.382
10	20 October 2013	08:50:03.97	32.8811	35.6019	0.2	0.621
11	20 October 2013	09:09:23.48	32.814	35.5327	3.7	0.407
12	20 October 2013	12:54:06.42	32.8659	35.5961	0.2	0.55
13	22 October 2013	03:53:25.05	32.9123	35.7012	0.2	0.37
14	22 October 2013	05:40:50.44	32.8566	35.6098	0.2	0.642
15	22 October 2013	08:23:40.50	32.7739	35.507	2	0.337
16	22 October 2013	08:53:22.61	32.7738	35.5113	6.2	0.344
17	29 October 2013	22:56:13.52	32.8982	35.6014	0.2	0.365
18	29 November 2013	12:21:35.23	32.7516	35.4968	5.7	0.377
19	3 December 2013	08:46:31.00	32.8664	35.6987	0.6	0.506
20	7 June 2018	23:47:19.55	32.751	35.5704	8.1	0.366
21	9 June 2018	02:29:16.22	32.7634	35.6252	8.4	0.369
22	2 July 2018	05:59:34.98	32.8592	35.6579	0.2	0.384
23	4 July 2018	01:50:06.67	32.9096	35.7	0.2	0.43
24	4 July 2018	01:54:26.53	32.8482	35.6202	8	0.315
25	4 July 2018	01:58:13.35	32.8594	35.6024	0.5	0.512
26	4 July 2018	03:41:21.65	32.8523	35.5979	0.4	0.38
27	4 July 2018	03:51:59.34	32.876	35.5836	0.3	0.493
28	4 July 2018	03:57:39.25	32.8523	35.5968	0.3	0.43
29	4 July 2018	04:19:17.36	32.869	35.5749	0.3	0.439
30	4 July 2018	05:22:37.08	32.8817	35.6564	0.2	0.348
31	4 July 2018	05:57:22.44	32.868	35.578	0.7	0.476
32	4 July 2018	12:29:07.00	32.8485	35.6074	0.2	0.409
33	4 July 2018	17:35:09.91	32.8526	35.4943	5.3	0.404
34	4 July 2018	19:45:39.34	32.8401	35.621	0.4	0.48
35	4 July 2018	19:51:24.20	32.8534	35.5904	0.3	0.408
36	4 July 2018	20:08:29.58	32.8632	35.5961	0.4	0.465
37	4 July 2018	20:14:56.92	32.8648	35.6047	0.2	0.492
38	4 July 2018	21:49:26.22	32.8889	35.5744	0.2	0.513
39	5 July 2018	01:24:47.37	32.8427	35.6275	0.2	0.374
40	5 July 2018	04:00:03.96	32.8642	35.5897	0.4	0.503
41	5 July 2018	04:30:25.21	32.884	35.5913	0.2	0.463
42	5 July 2018	07:08:23.50	32.8762	35.574	4.6	0.382
43	5 July 2018	08:29:53.90	32.8514	35.5957	0.2	0.418

44	5 July 2018	09:02:54.13	32.9252	35.692	0.6	0.374
45	5 July 2018	09:40:59.02	32.7528	35.5256	0.3	0.393
46	5 July 2018	10:04:30.00	32.8632	35.5939	0.3	0.514
47	5 July 2018	16:51:36.99	32.8486	35.6448	0.2	0.323
48	5 July 2018	19:43:55.20	32.8715	35.5407	1.2	0.347
49	5 July 2018	20:41:06.37	32.8301	35.6239	0.2	0.438
50	5 July 2018	23:20:38.38	32.8589	35.5853	0.2	0.535
51	5 July 2018	23:56:56.65	32.8947	35.598	0.2	0.421
52	6 July 2018	00:55:10.45	32.8765	35.5633	0.7	0.436
53	6 July 2018	01:06:10.22	32.8704	35.5931	0.2	0.439
54	6 July 2018	01:38:50.10	32.8676	35.6015	0.4	0.387
55	6 July 2018	02:07:44.38	32.8521	35.6086	0.2	0.53
56	6 July 2018	05:38:54.23	32.8776	35.5954	0.3	0.333
57	6 July 2018	10:08:48.44	32.8917	35.5659	4.8	0.395
58	6 July 2018	17:13:24.17	32.8784	35.5986	2.9	0.4
59	6 July 2018	20:20:45.64	32.8379	35.5985	1.9	0.389
60	6 July 2018	22:54:46.64	32.8896	35.5829	0.8	0.376
61	7 July 2018	11:46:31.59	32.8604	35.6003	0.8	0.494
62	7 July 2018	17:33:27.09	32.8606	35.5896	0.3	0.399
63	7 July 2018	18:28:25.26	32.9019	35.5544	4	0.351
64	8 July 2018	11:04:01.55	32.8668	35.594	0.2	0.581
65	8 July 2018	12:39:10.22	32.9088	35.5707	0.3	0.42
66	8 July 2018	12:52:17.38	32.8569	35.5927	0.2	0.4
67	8 July 2018	13:30:47.85	32.8513	35.6043	0.2	0.514
68	8 July 2018	13:53:54.87	32.8611	35.6067	0.2	0.424
69	8 July 2018	14:22:01.46	32.8502	35.6106	0.2	0.399
70	8 July 2018	14:51:40.77	32.8514	35.6395	0.2	0.458
71	8 July 2018	18:36:51.13	32.8667	35.6004	0.4	0.392
72	8 July 2018	19:00:48.29	32.8597	35.5906	0.8	0.523
73	8 July 2018	20:04:54.05	32.8656	35.563	0.4	0.454
74	8 July 2018	21:42:45.26	32.8522	35.6032	0.2	0.569
75	8 July 2018	21:56:45.19	32.8101	35.5902	1.6	0.381
76	9 July 2018	00:59:30.27	32.8603	35.6024	0.4	0.509
77	9 July 2018	02:45:23.95	32.8546	35.6182	0.3	0.545
78	9 July 2018	05:19:40.93	32.8729	35.607	2.1	0.368
79	9 July 2018	05:26:40.02	32.8821	35.5966	0.2	0.356
80	9 July 2018	05:45:24.56	32.8463	35.6255	0.2	0.418
81	9 July 2018	06:01:12.78	32.8397	35.5975	0.2	0.491
82	9 July 2018	15:16:05.47	32.8646	35.6121	0.2	0.511
83	10 July 2018	19:25:20.38	32.8467	35.6063	0.2	0.42
84	10 July 2018	23:04:15.56	32.8827	35.5656	0.3	0.354
85	11 July 2018	00:21:09.02	32.8368	35.6081	0.2	0.422
86	11 July 2018	07:51:38.05	32.8704	35.5931	0.7	0.364
87	11 July 2018	20:01:04.06	32.8898	35.5744	0.2	0.337
88	12 July 2018	07:00:35.03	32.8752	35.6231	0.2	0.434
89	12 July 2018	11:02:53.30	32.8656	35.5673	0.2	0.417

90	12 July 2018	11:43:06.71	32.8224	35.6056	0.2	0.392
91	13 July 2018	00:11:43.35	32.8832	35.5849	0.7	0.419
92	13 July 2018	06:06:45.00	32.8972	35.6045	1.4	0.319
93	14 July 2018	17:11:46.58	32.8275	35.6196	0.5	0.365
94	15 July 2018	14:03:33.18	32.8743	35.5814	2.1	0.393
95	16 July 2018	20:33:17.58	32.921	35.4994	0.2	0.358
96	18 July 2018	15:24:09.15	32.8789	35.5784	0.5	0.389
97	22 July 2018	06:41:26.13	32.8477	35.6042	0.2	0.543
98	25 July 2018	10:52:05.26	32.8813	35.5923	0.2	0.384
99	26 July 2018	17:52:28.69	32.7599	35.4874	1.7	0.341
100	27 July 2018	08:51:18.03	32.8651	35.5886	0.3	0.482
101	27 July 2018	10:12:04.84	32.8754	35.5718	0.2	0.415
102	27 July 2018	11:56:37.10	32.8815	35.5378	0.2	0.439
103	28 July 2018	23:49:38.07	32.8833	35.5838	3.8	0.463
104	29 July 2018	00:07:54.80	32.8932	35.5841	0.2	0.429
105	29 July 2018	00:26:59.07	32.8787	35.5848	1.4	0.412
106	29 July 2018	08:46:42.43	32.8156	35.6278	3	0.393
107	29 July 2018	11:59:51.02	32.761	35.5195	2.4	0.389
108	30 July 2018	02:59:49.03	32.8383	35.6199	0.4	0.389
109	31 July 2018	00:42:56.52	32.8371	35.6338	0.3	0.457
110	31 July 2018	16:25:27.87	32.88	35.6083	5.8	0.401
111	4 August 2018	03:07:10.54	32.902	35.5491	1.4	0.437
112	5 August 2018	00:44:34.31	32.8631	35.6014	0.4	0.364
113	5 August 2018	01:33:02.14	32.8309	35.6314	0.2	0.418
114	8 August 2018	22:10:28.14	32.8555	35.6161	2.6	0.485
115	8 August 2018	23:21:09.80	32.8437	35.6201	2.1	0.418
116	10 August 2018	14:40:48.81	32.8385	35.6124	0.7	0.458
117	13 August 2018	05:56:48.93	32.7991	35.5536	3.5	0.436
118	17 August 2018	02:40:55.03	32.9047	35.6774	0.2	0.343
119	17 August 2018	07:53:09.42	32.8482	35.6223	0.2	0.399

Table S1. Relocation results using Grigoli et al.'s (2013) method. Only results with low location uncertainty were considered (misfit <0.65). Uncertainties are ±3 km.

The seven normal earthquakes mechanism solutions

No.	Date	Time (hour: minute: second)	Location		Depth (km)	Strike (°)	Dip (°)	Rake (°)	Mw
			Lat. (°N)	Long. (°E)					
1	17 October 2013	18:17:53	32.85	35.56	4.6	173/330	34/58	-070/-103	3.3
2	20 October 2013	08:50:03	32.85	35.56	5.8	173/338	39/52	-079/-099	3.6
3	4 July 2018	01:50:06	32.84	35.58	4.1	150/327	31/59	-087/-092	4.1
4	4 July 2018	03:51:59	32.84	35.57	5.0	166/338	42/48	-084/-095	3.9
5	4 July 2018	19:45:39	32.85	35.58	4.7	152/317	42/49	-079/-100	4.5
6	8 July 2018	13:30:47	32.84	35.59	5.1	158/307	44/50	-067/-111	3.9
7	27 July 2018	08:51:18	32.87	35.57	3.4	010/174	65/25	-083/-105	3.7

Table S2. Results of point source parameters for the seven largest earthquakes using Cesca et al.'s (2010) method. Mw – Moment magnitude.

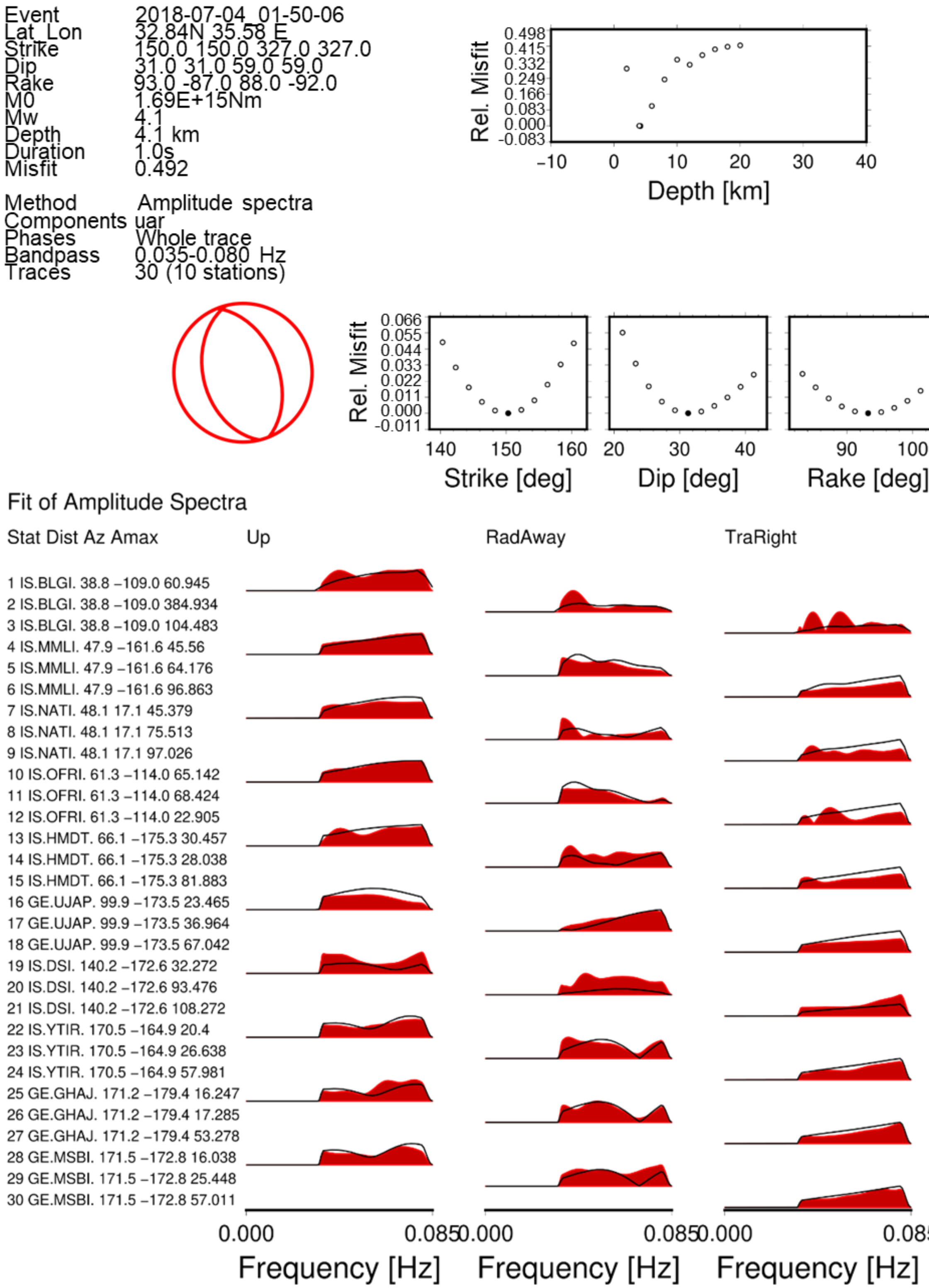
Event 2018-07-04_01-50-06
Lat_Lon 32.84N 35.58 E
Strike 150.0 150.0 327.0 327.0
Dip 31.0 31.0 59.0 59.0
Rake 93.0 -87.0 88.0 -92.0
M0 1.69E+15Nm
Mw 4.1
Depth 4.1 km
Duration 1.0s
Misfit 0.492
Method Amplitude spectra
Components uar
Phases Whole trace
Bandpass 0.035-0.080 Hz
Traces 30 (10 stations)
Rel. Misfit
Depth [km]
Strike [deg]
Dip [deg]
Rake [deg]
Fit of Amplitude Spectra
Stat Dist Az Amax
Up
RadAway
TraRight
1 IS.BLGI. 38.8 −109.0 60.945
2 IS.BLGI. 38.8 −109.0 384.934
3 IS.BLGI. 38.8 −109.0 104.483
4 IS.MMLI. 47.9 −161.6 45.56
5 IS.MMLI. 47.9 −161.6 64.176
6 IS.MMLI. 47.9 −161.6 96.863
7 IS.NATI. 48.1 17.1 45.379
8 IS.NATI. 48.1 17.1 75.513
9 IS.NATI. 48.1 17.1 97.026
10 IS.OFRI. 61.3 −114.0 65.142
11 IS.OFRI. 61.3 −114.0 68.424
12 IS.OFRI. 61.3 −114.0 22.905
13 IS.HMDT. 66.1 −175.3 30.457
14 IS.HMDT. 66.1 −175.3 28.038
15 IS.HMDT. 66.1 −175.3 81.883
16 GE.UJAP. 99.9 −173.5 23.465
17 GE.UJAP. 99.9 −173.5 36.964
18 GE.UJAP. 99.9 −173.5 67.042
19 IS.DSI. 140.2 −172.6 32.272
20 IS.DSI. 140.2 −172.6 93.476
21 IS.DSI. 140.2 −172.6 108.272
22 IS.YTIR. 170.5 −164.9 20.4
23 IS.YTIR. 170.5 −164.9 26.638
24 IS.YTIR. 170.5 −164.9 57.981
25 GE.GHAJ. 171.2 −179.4 16.247
26 GE.GHAJ. 171.2 −179.4 17.285
27 GE.GHAJ. 171.2 −179.4 53.278
28 GE.MSBI. 171.5 −172.8 16.038
29 GE.MSBI. 171.5 −172.8 25.448
30 GE.MSBI. 171.5 −172.8 57.011
Frequency [Hz]
Frequency [Hz]
Frequency [Hz]

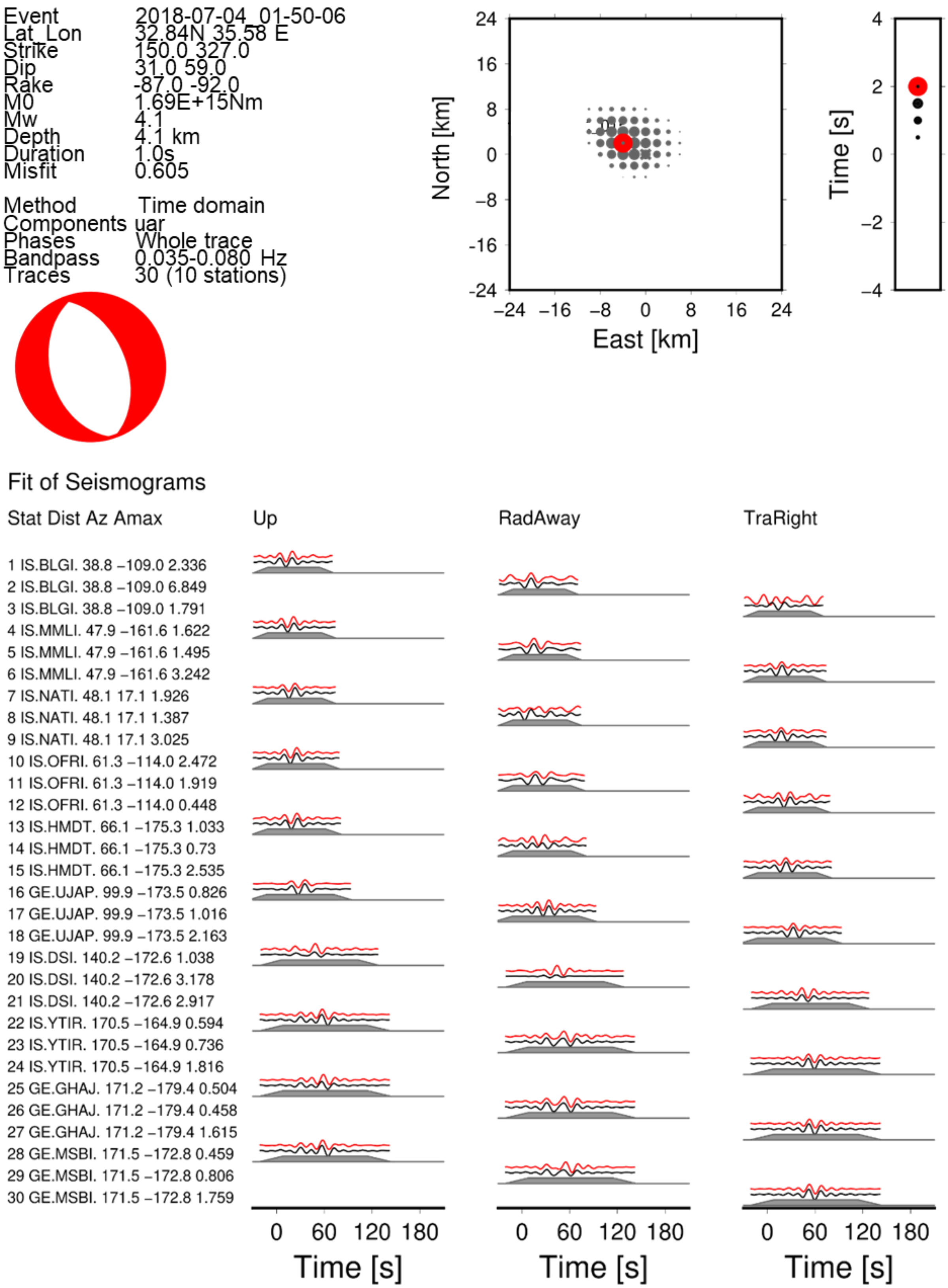

Figure S1. Focal mechanism, magnitude, and centroid location using Cesca et al.'s (2010) method of the 4th of July 2018 Mw 4.1 (Table 1). Uncertainties estimated ±3 km.

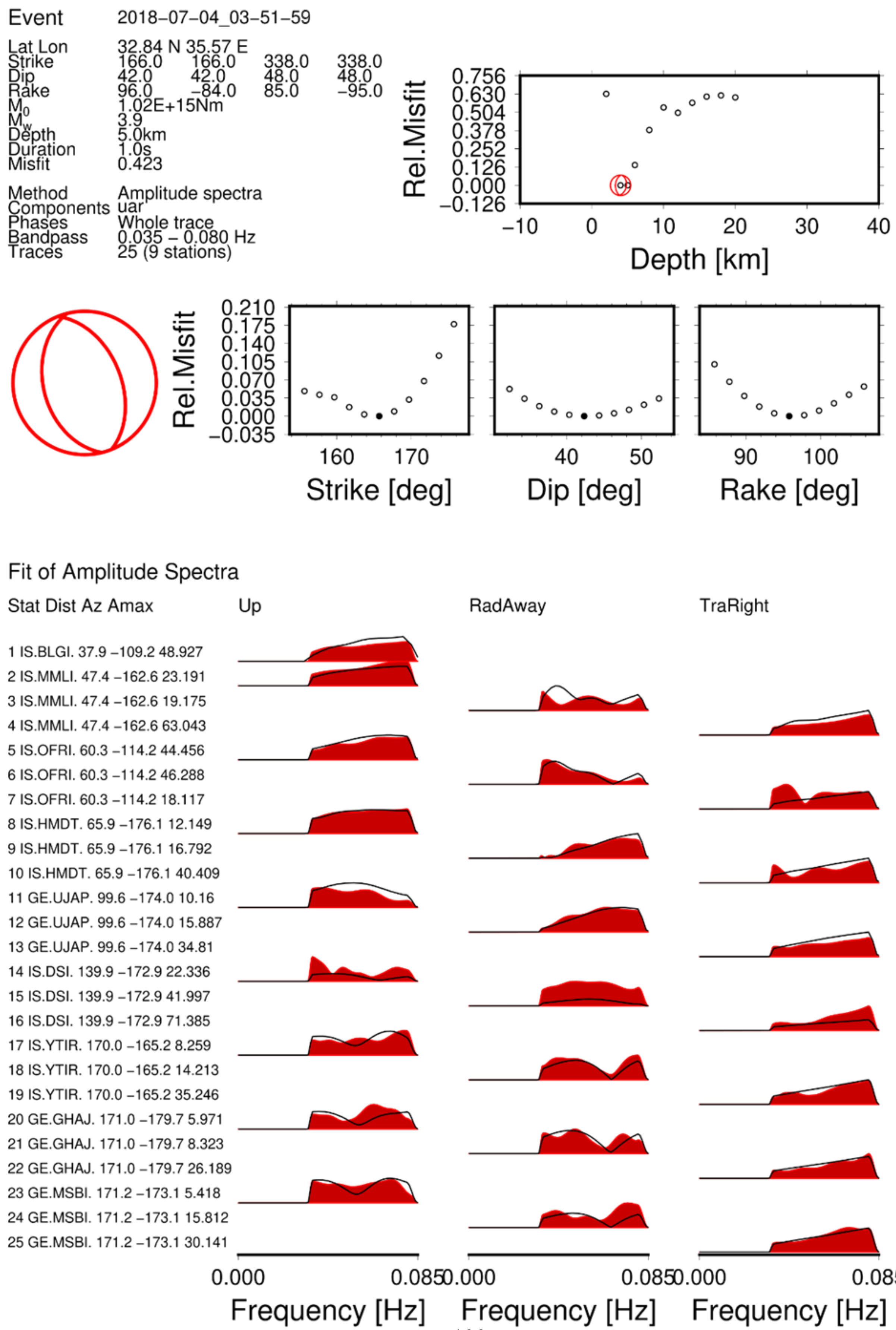
Event 2018–07–04_03–51–59
Lat Lon 32.84 N 35.57 E
Strike 166.0 166.0 338.0 338.0
Dip 42.0 42.0 48.0 48.0
Rake 96.0 –84.0 85.0 –95.0
M0 1.02E+15Nm
Mw 3.9
Depth 5.0km
Duration 1.0s
Misfit 0.423
Method Amplitude spectra
Components uar
Phases Whole trace
Bandpass 0.035 – 0.080 Hz
Traces 25 (9 stations)
Rel.Misfit
Depth [km]
Strike [deg]
Dip [deg]
Rake [deg]
Fit of Amplitude Spectra
Stat Dist Az Amax
Up
RadAway
TraRight
1 IS.BLGI. 37.9 –109.2 48.927
2 IS.MMLI. 47.4 –162.6 23.191
3 IS.MMLI. 47.4 –162.6 19.175
4 IS.MMLI. 47.4 –162.6 63.043
5 IS.OFRI. 60.3 –114.2 44.456
6 IS.OFRI. 60.3 –114.2 46.288
7 IS.OFRI. 60.3 –114.2 18.117
8 IS.HMDT. 65.9 –176.1 12.149
9 IS.HMDT. 65.9 –176.1 16.792
10 IS.HMDT. 65.9 –176.1 40.409
11 GE.UJAP. 99.6 –174.0 10.16
12 GE.UJAP. 99.6 –174.0 15.887
13 GE.UJAP. 99.6 –174.0 34.81
14 IS.DSI. 139.9 –172.9 22.336
15 IS.DSI. 139.9 –172.9 41.997
16 IS.DSI. 139.9 –172.9 71.385
17 IS.YTIR. 170.0 –165.2 8.259
18 IS.YTIR. 170.0 –165.2 14.213
19 IS.YTIR. 170.0 –165.2 35.246
20 GE.GHAJ. 171.0 –179.7 5.971
21 GE.GHAJ. 171.0 –179.7 8.323
22 GE.GHAJ. 171.0 –179.7 26.189
23 GE.MSBI. 171.2 –173.1 5.418
24 GE.MSBI. 171.2 –173.1 15.812
25 GE.MSBI. 171.2 –173.1 30.141
Frequency [Hz]

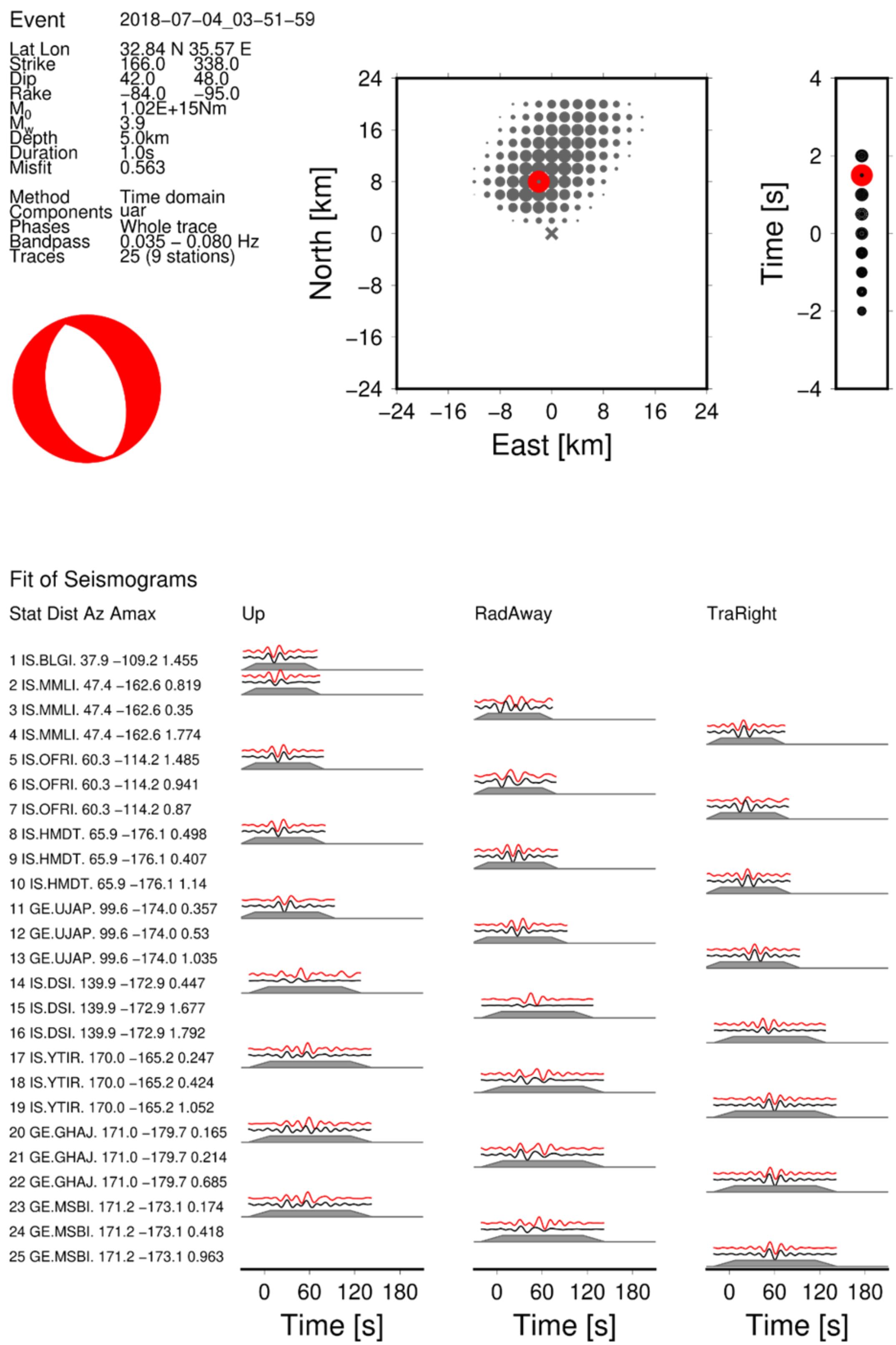

Figure S2 Focal mechanism, magnitude, and centroid location using Cesca et al.'s (2010) method of the 4th of July 2018 Mw 3.9 (Table 1). Uncertainties estimated ±3 km.

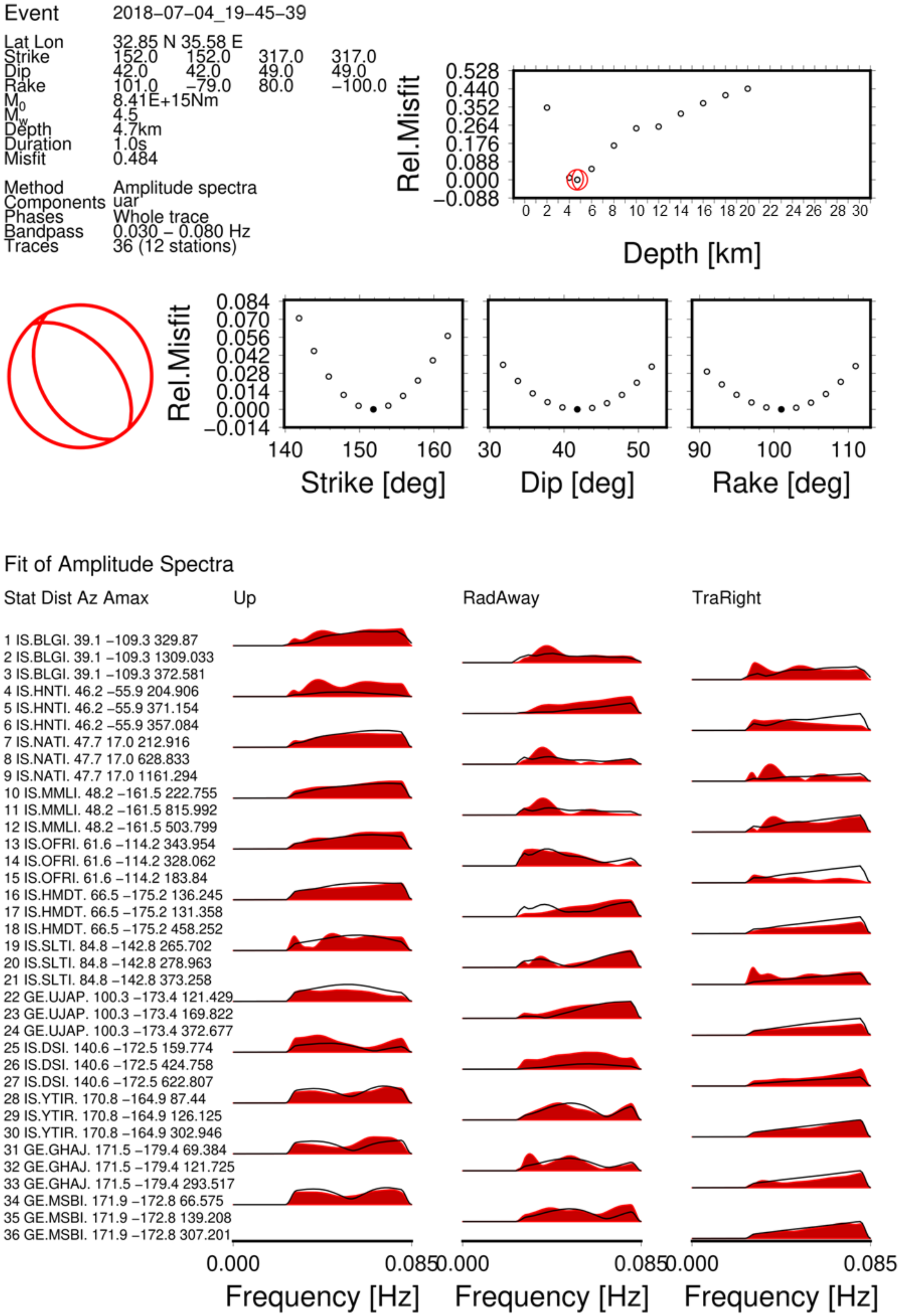
Event 2018-07-04_19-45-39
Lat Lon 32.85 N 35.58 E
Strike 152.0 152.0 317.0 317.0
Dip 42.0 42.0 49.0 49.0
Rake 101.0 −79.0 80.0 −100.0
M0 8.41E+15Nm
Mw 4.5
Depth 4.7km
Duration 1.0s
Misfit 0.484
Method Amplitude spectra
Components uar
Phases Whole trace
Bandpass 0.030 – 0.080 Hz
Traces 36 (12 stations)
Rel.Misfit
Depth [km]
Strike [deg]
Dip [deg]
Rake [deg]
Fit of Amplitude Spectra
Stat Dist Az Amax
Up
RadAway
TraRight
1 IS.BLGI. 39.1 −109.3 329.87
2 IS.BLGI. 39.1 −109.3 1309.033
3 IS.BLGI. 39.1 −109.3 372.581
4 IS.HNTI. 46.2 −55.9 204.906
5 IS.HNTI. 46.2 −55.9 371.154
6 IS.HNTI. 46.2 −55.9 357.084
7 IS.NATI. 47.7 17.0 212.916
8 IS.NATI. 47.7 17.0 628.833
9 IS.NATI. 47.7 17.0 1161.294
10 IS.MMLI. 48.2 −161.5 222.755
11 IS.MMLI. 48.2 −161.5 815.992
12 IS.MMLI. 48.2 −161.5 503.799
13 IS.OFRI. 61.6 −114.2 343.954
14 IS.OFRI. 61.6 −114.2 328.062
15 IS.OFRI. 61.6 −114.2 183.84
16 IS.HMDT. 66.5 −175.2 136.245
17 IS.HMDT. 66.5 −175.2 131.358
18 IS.HMDT. 66.5 −175.2 458.252
19 IS.SLTI. 84.8 −142.8 265.702
20 IS.SLTI. 84.8 −142.8 278.963
21 IS.SLTI. 84.8 −142.8 373.258
22 GE.UJAP. 100.3 −173.4 121.429
23 GE.UJAP. 100.3 −173.4 169.822
24 GE.UJAP. 100.3 −173.4 372.677
25 IS.DSI. 140.6 −172.5 159.774
26 IS.DSI. 140.6 −172.5 424.758
27 IS.DSI. 140.6 −172.5 622.807
28 IS.YTIR. 170.8 −164.9 87.44
29 IS.YTIR. 170.8 −164.9 126.125
30 IS.YTIR. 170.8 −164.9 302.946
31 GE.GHAJ. 171.5 −179.4 69.384
32 GE.GHAJ. 171.5 −179.4 121.725
33 GE.GHAJ. 171.5 −179.4 293.517
34 GE.MSBI. 171.9 −172.8 66.575
35 GE.MSBI. 171.9 −172.8 139.208
36 GE.MSBI. 171.9 −172.8 307.201
Frequency [Hz]
Frequency [Hz]
Frequency [Hz]

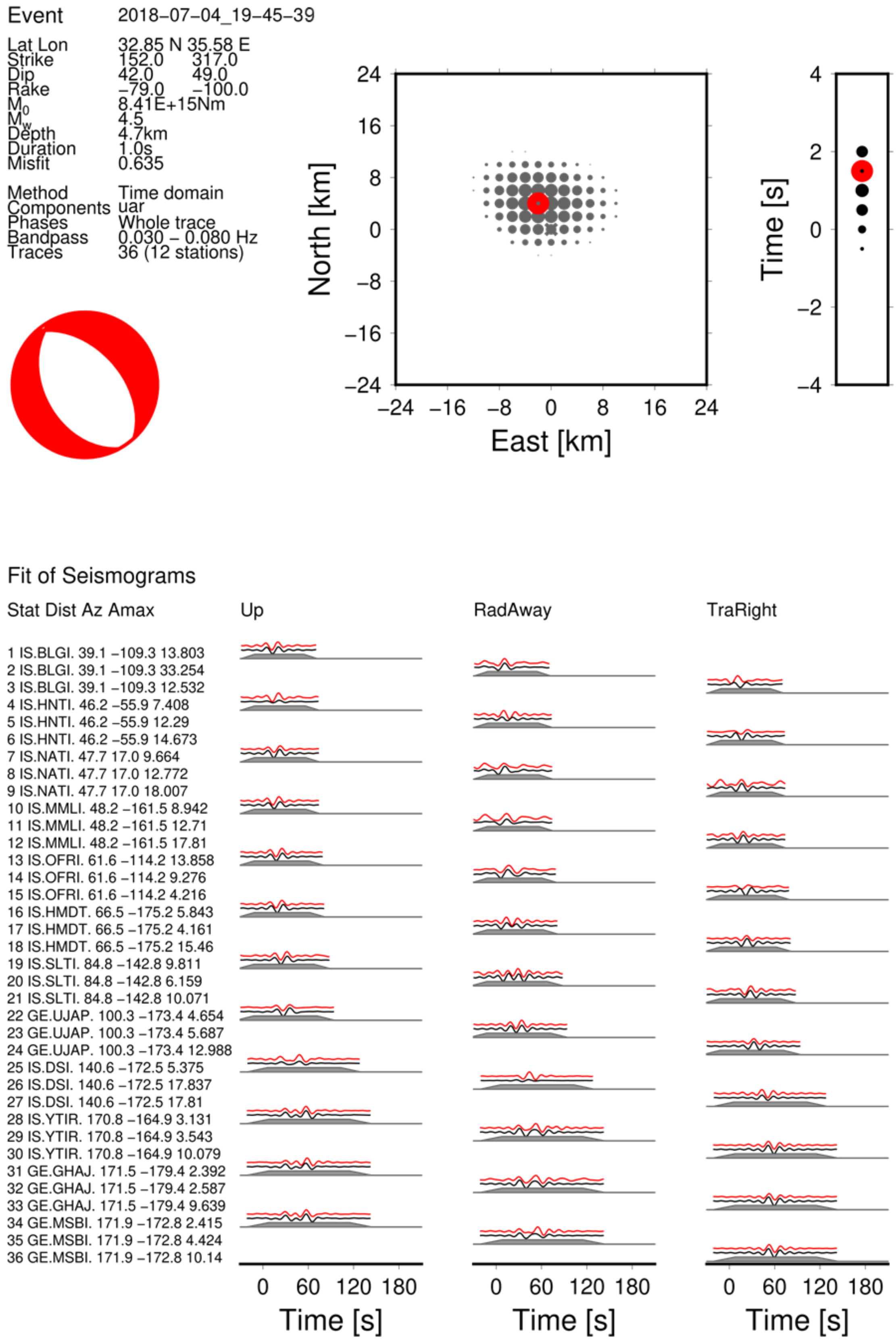

Figure S3 Focal mechanism, magnitude, and centroid location using Cesca et al.'s (2010) method of the 4th of July 2018 Mw 4.5 (Table 1). Uncertainties estimated ±3 km.

Earthquake (Year-Month-Day hour:minute)	Station	Ts-Tp (s)	Depth (km) based on local Ts-Tp modeling(1)		Depth estimates in this and previous studies (km)			
			Modeling Ts-Tp(2)	Modeling Ts-Tp(3)	Centroid depth (this study)	Centroid depth (Haddad et al. 2020)	Hypocenter depth (Haddad et al. 2020)	Hypocenter depth (ISN catalog, earthquake.co.il)
2018-07-04 01:49	K10B	1.46	7.5	6.9	4.1	3.0	9.8	4
2018-07-04 03:51	K10B	1.54	8.6	7.9	5.0	n.a.	10.9	5
2018-07-04 19:45	K10B	1.60	8.1	8.8	4.7	3.0	11.4	6

(1) assuming velocity model by Haddad et al. (2020)

(2) assuming epicentral locations in this study

(3) assuming epicentral locations by Haddad et al. (2020)

Table S3. Depth calculations of three earthquakes using K10B borehole records (location in Fig. 3a) with Haddad et al. (2020) results and our study results.

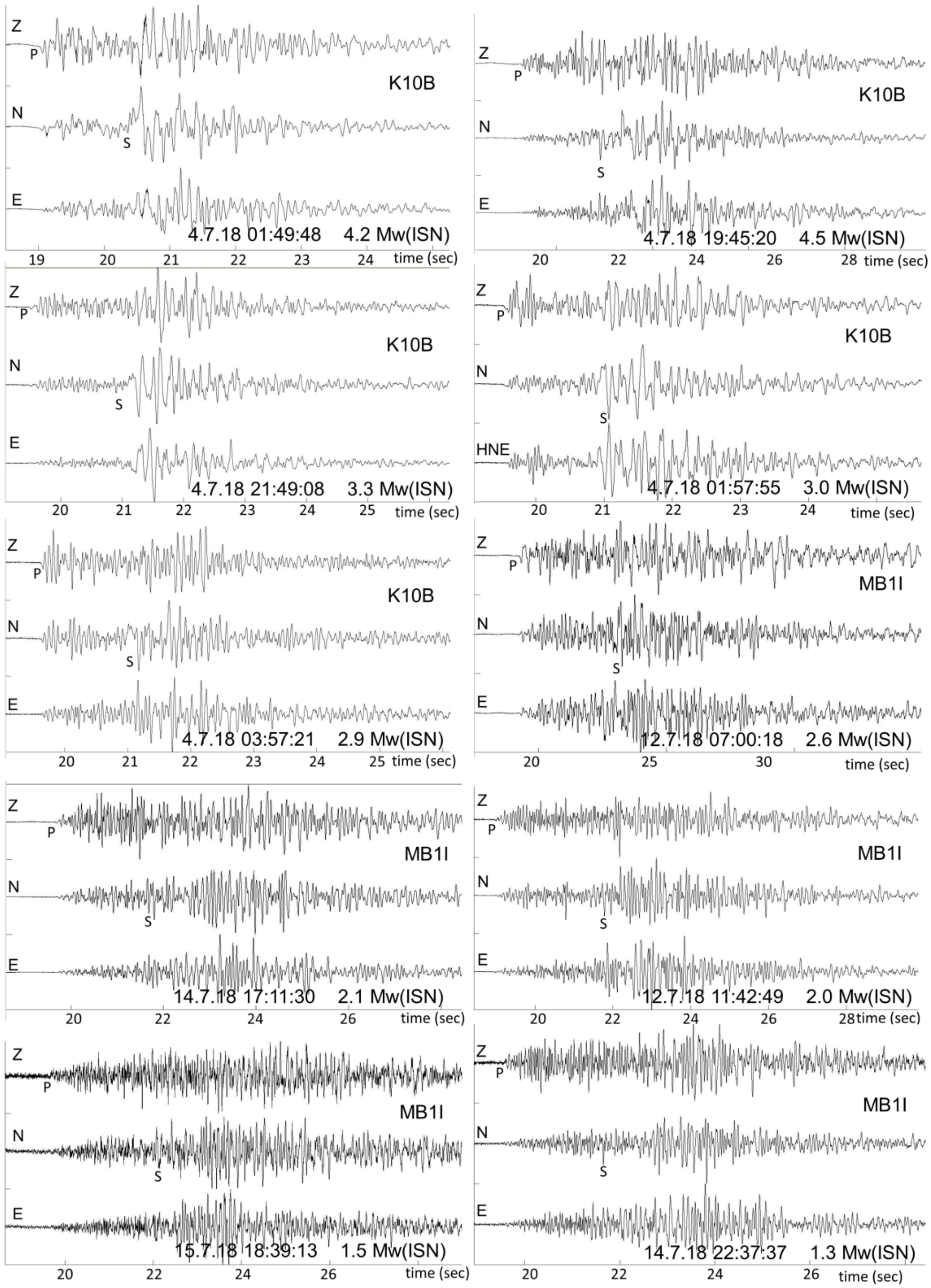

Figure S4. Examples of earthquakes recorded in boreholes (location in Fig. 4). For each earthquake the three components are shown (Z, N, E) with relative time. For every earthquake at the top right - the name of the station. Bottom right - date recorded, time (hour: minute: second) and Mw according to the ISN (Israel Seismic Network).

Event (Date, time)	Model	Mw		Depth (km)		CLVD (%)	ISO (%)
		DC	MT	DC	MT	MT	MT
17.10.2013 18:17	Crust_T4	3.34±0.06	3.42±0.07	3.9±1.9	9.0±3.0	+4±22	+46±18
	Gittermann_2002	3.43±0.07	3.42±0.05	2.2±1.4	6.1±3.4	0±30	+26±25
	Haddad_2020	3.21±0.05	3.27±0.06	2.8±1.4	6.5±2.8	-5±24	+42±20
20.10.2013 08:50	Crust_T4	3.62±0.06	3.71±0.07	5.1±3.9	8.6±2.8	-13±18	+41±10
	Gittermann_2002	3.64±0.06	3.69±0.06	3.3±2.5	6.1±4.0	-15±26	+23±22
	Haddad_2020	3.51±0.08	3.56±0.09	4.2±4.3	6.4±4.2	-14±22	+29±23
04.07.2018 01:50	Crust_T4	4.00±0.02	4.01±0.02	3.0±0.3	4.1±0.4	+13±9	+29±7
	Gittermann_2002	4.06±0.02	4.03±0.03	2.8±0.4	3.3±0.5	+11±13	+21±12
	Haddad_2020	3.90±0.02	3.91±0.03	2.1±0.3	2.9±0.5	-1±15	+22±15
04.07.2018 03:51	Crust_T4	3.93±0.05	3.94±0.06	3.8±0.6	6.1±1.8	+17±16	+32±13
	Gittermann2002	3.96±0.04	3.96±0.07	3.4±0.6	3.9±1.2	+7±22	+8±17
	Haddad2020	3.79±0.03	3.81±0.04	2.9±0.4	3.7±1.3	+1±13	+21±14
04.07.2018 19:45	Crust_T4	4.53±0.03	4.53±0.02	3.5±0.6	4.4±0.6	+7±11	+22±10
	Gittermann_2002	4.56±0.02	4.55±0.03	3.1±0.4	3.8±0.6	+10±13	+16±13
	Haddad_2020	4.41±0.02	4.41±0.02	2.7±0.5	3.1±0.3	-7±10	+13±7
08.07.2018 13:30	Crust_T4	3.88±0.04	3.87±0.04	3.8±0.5	4.6±0.6	+9±13	+23±11
	Gittermann_2002	3.91±0.03	3.89±0.03	3.5±0.6	3.9±0.7	+13±17	+17±14
	Haddad_2020	3.77±0.03	3.76±0.03	2.7±0.5	3.5±0.8	+5±16	+20±14
27.07.2018 08:51	Crust_T4	3.56±0.05	3.58±0.06	5.0±5.7	5.9±5.3	-1±23	+26±17
	Gittermann_2002	3.60±0.05	3.63±0.05	2.9±2.9	4.5±2.0	+15±20	+33±16
	Haddad_2020	3.51±0.07	3.55±0.11	6.4±7.8	6.1±5.9	+1±23	+31±19

Table S4. Summary of double couple and moment tensor inversion results. The table reports mean values and standard deviations for Mw, depth, compensated linear vector dipole (CLVD) and isotropic percentage (ISO), as obtained using the Grond software (Heimann et al., 2018) by fitting simultaneously full waveform and amplitude spectra for the 7 considered earthquakes and 3 velocity models: Crust_T4 (regional model from the CRUST2.0 database, http://igppweb.ucsd.edu/~gabi/rem.html), Gittermann_2002 (Gitterman et al., 2002), Haddad_2020 (Haddad et al., 2020).

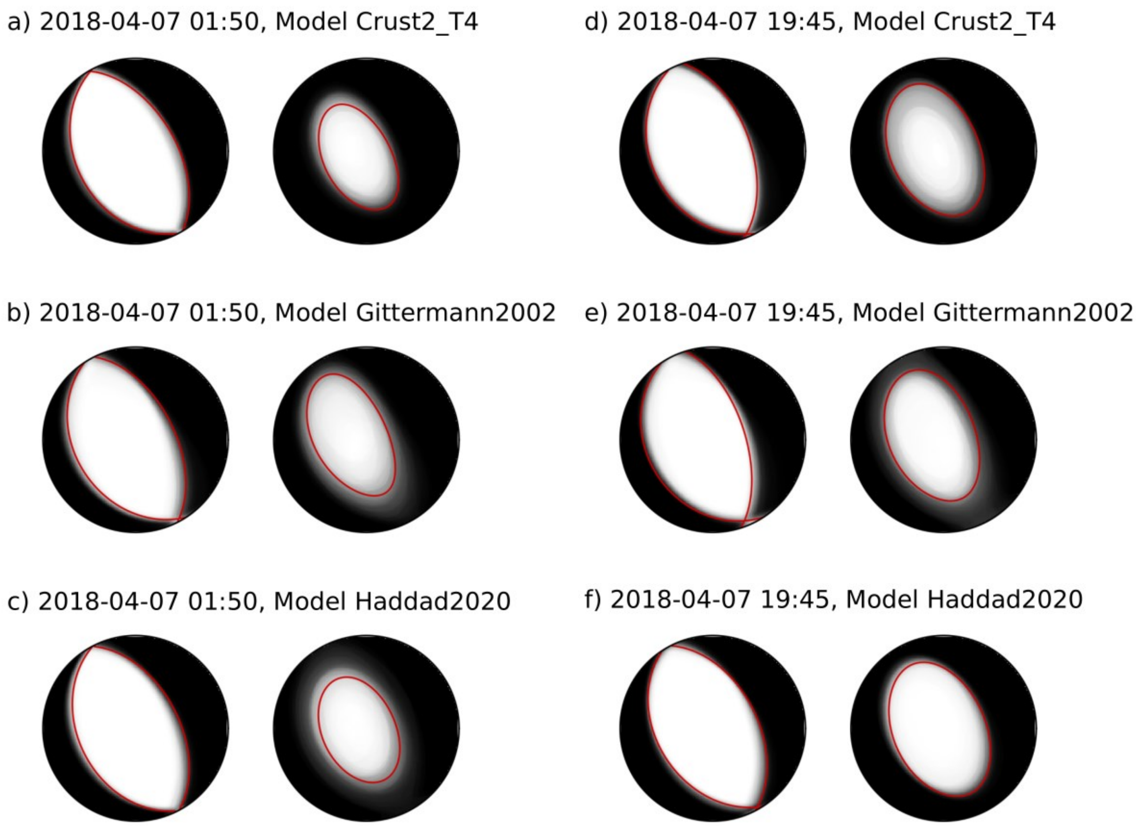

Figure S5. Comparison of moment tensor solutions and uncertainties. Fuzzy focal spheres, plotted as the overlay of semitransparent solutions for different bootstrap chains, are illustrative of the stability of the moment tensor solutions. Different panels correspond to double-couple (DC) versus full moment tensors (MT) as obtained using the Grond software (Heimann et al., 2018) by fitting simultaneously full waveform and amplitude spectra for the two largest considered earthquakes and three velocity models: Crust_T4 (regional model from the CRUST2.0 database, http://igppweb.ucsd.edu/~gabi/rem.html), Gittermann_2002 (Gitterman et al., 2002) and Haddad_2020 (Haddad et al., 2020). Red lines in each plot denote the best solution.

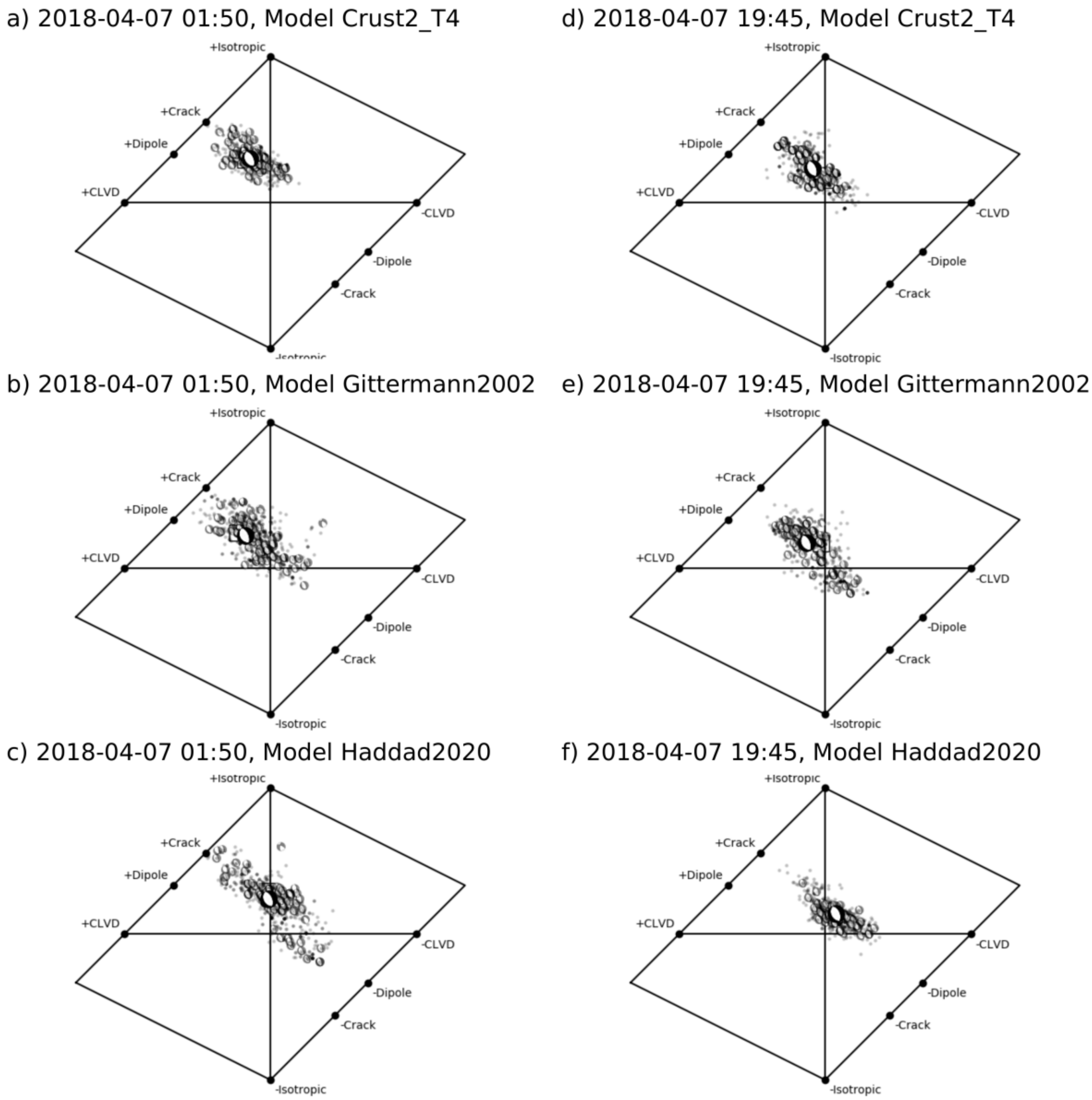

Figure S6. Comparison of moment tensor decomposition and uncertainties. Hudson plots (Hudson et al., 1989) illustrate the moment tensor decomposition, as obtained using the Grond software (Heimann et al., 2018) by performing a full moment tensor inversion, fitting simultaneously full waveform and amplitude spectra for the two largest considered earthquakes and three velocity models: Crust_T4 (regional model from the CRUST2.0 database, http://igppweb.ucsd.edu/~gabi/rem.html), Gittermann_2002 (Gitterman et al., 2002) and Haddad_2020 (Haddad et al., 2020). In each plot, moment tensor ensembles result from different bootstrap chains, with less transparent focal spheres corresponding to best solutions. The mean solution of the different bootstrap chains is represented by a larger focal sphere, while the best solution, using all data, by a black square.

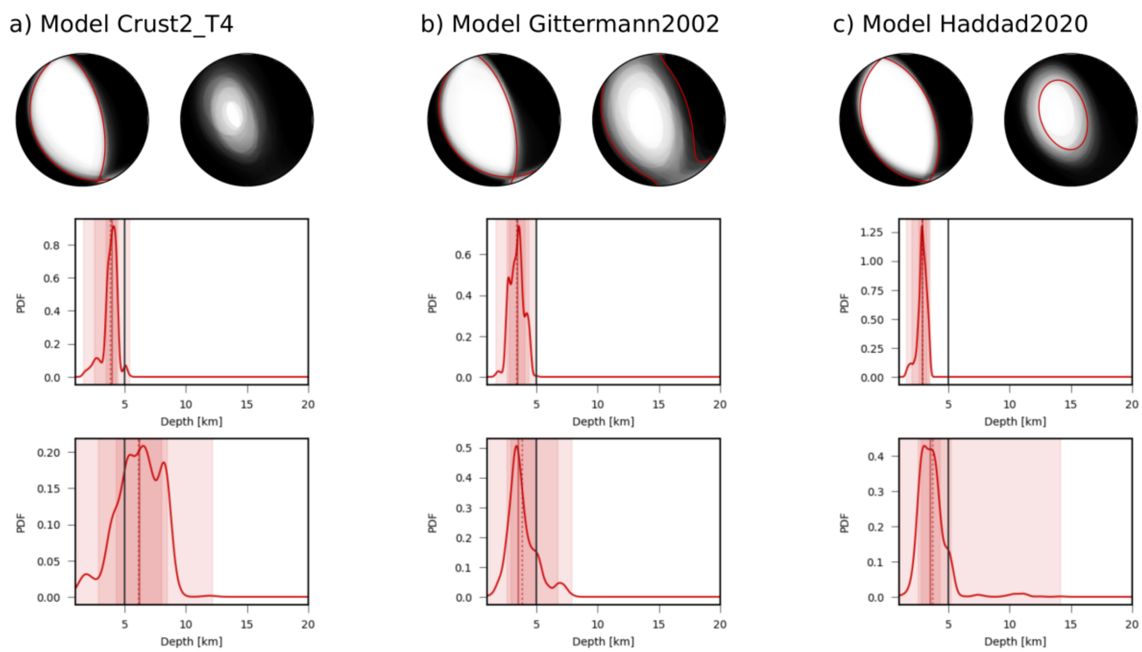

Figure S7. Details of the MT inversion result for the earthquake on 4.7.2018, 03:51. The figure illustrates the centroid moment tensor result as obtained using the Grond software (Heimann et al., 2018) by performing double couple and full moment tensor inversion, fitting simultaneously full waveform and amplitude spectra for three velocity models: a, Crust_T4 (regional model from the CRUST2.0 database, http://igppweb.ucsd.edu/~gabi/rem.html), b, Gittermann_2002 (Gitterman et al., 2002) and c, Haddad_2020 (Haddad et al., 2020). For each model, we report: fuzzy focal spheres, plotted as the overlay of semitransparent solutions for different bootstrap chains, illustrative of the stability of the double couple and full moment tensor solutions, with red lines denoting the best solution (top) and depth histograms for the double couple and full moment tensor inversion (bottom); here a black line denotes the reference inversion, as described in the main manuscript, a solid red line the mean solution, a dashed red line the best solution, dark, medium and light pink regions represent respectively the 68% confidence interval, 90% confidence interval and whole range of solutions out of the bootstrap test.

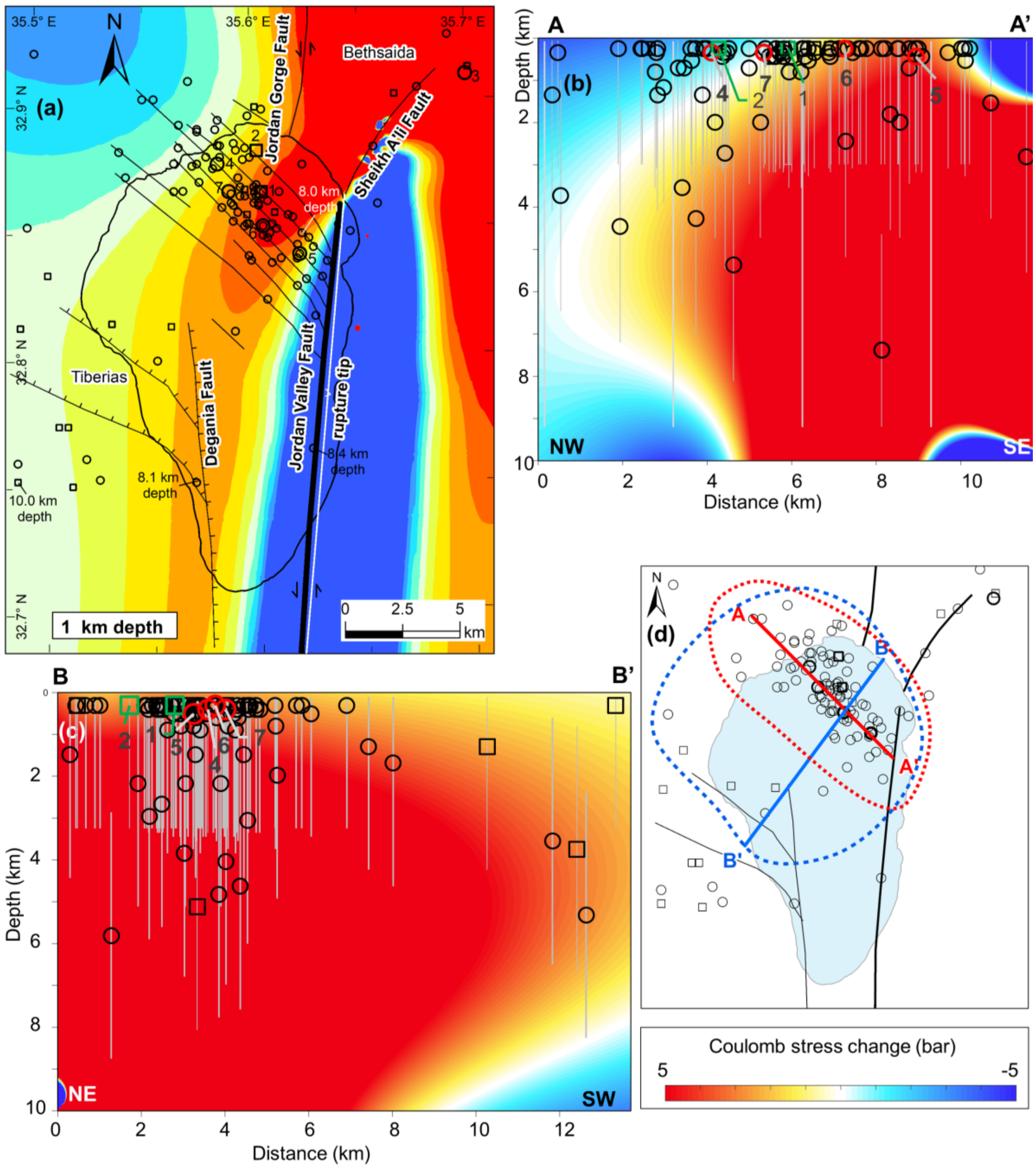

Figure S8. Coulomb stress change model considering accumulated slip on the Jordan Valley Fault since the 1759 CE earthquake. **(a)** Depth slice of 1 km. The 2013 (rectangles) and 2018 (circles) relocated hypocenters are marked. The seven largest earthquakes are in bold. (b-c) Coulomb stress change cross-sections. The seven larger earthquakes (no. 1-7) are colored. See Table S2 for additional details. **(b)** A-A' cross-section (NW-SE direction). The larger earthquakes are marked. A depth error of ±3 km is estimated as in Grigoli et al. (2013). **(c)** B-B′ cross-section (NE-SW direction). **(d)** a map showing the location of the cross-sections. The earthquakes in the dashed red polygon are projected in (b). The earthquakes in the blue polygon are projected in (c).

References

Cesca, S., Heimann, S., Stammler, K., & Dahm, T. (2010). Automated procedure for point and kinematic source inversion at regional distances. *Geophysical Research*, *115*, 1–24. https://doi.org/10.1029/2009JB006450.

Gitterman, Y., Pinsky, V., Shapira, A., Ergin, M., Kalafat, D., Gurbuz, G., & Solomi, K. (2002). Improvement in detection, location and identification of small events through joint data analysis by seismic stations in the Middle East/Eastern Mediterranean region. *Proceedings of the 24th Seismic Research Review Nuclear Explosion Monitoring: Innovation and Integration*, 271–282. https://doi.org/DTRA01-00-C-0119.

Grigoli, F., Cesca, S., Vassallo, M., & Dahm, T. (2013). Automated Seismic Event Location by Travel-Time Stacking: An Application to Mining Induced Seismicity. *Seismological Research Letters*, *84*(4), 666–677. https://doi.org/10.1785/0220120191.

Haddad, A., Alcanie, M., Zahradník, J., Lazar, M., Antunes, V., Gasperini, L. et al. (2020). Tectonics of the Dead Sea Fault Driving the July 2018 Seismic Swarm in the Sea of Galilee (Lake Kinneret), Israel. *Journal of Geophysical Research: Solid Earth*, *125*(10), 1–14. https://doi.org/10.1029/2019jb018963.

Heimann, S., Isken, M., Kühn, D., Sudhaus, H., Steinberg, A., Vasyura-Bathke, Hannes Daout, S. et al. (2018). Grond - A probabilistic earthquake source inversion framework. V. 1.0. *GFZ Data Services*. https://doi.org/10.5880/GFZ.2.1.2018.003.

Hudson, J. A., Pearce, R. G., & Rogers, R. M. (1989). Source type plot for inversion of the moment tensor. *Journal of Geophysical Research: Solid Earth*, *94*(B1), 765–774. https://doi.org/10.1029/JB094iB01p00765; https://doi.org/10.1029/JB094iB01p00765.